AIAA 96-0330
Certification of a CFD Code for High-Speed Civil Transport Design Optimization

D.L. Knill, V. Balabanov,
B. Grossman, W.H. Mason
Virginia Polytechnic Institute and
State University, Blacksburg, VA

R.T. Haftka
University of Florida
Gainesville, FL

34th Aerospace Sciences Meeting & Exhibit
January 15-18, 1996 / Reno, NV

CERTIFICATION OF A CFD CODE FOR HIGH-SPEED CIVIL TRANSPORT DESIGN OPTIMIZATION

Duane L. Knill*, Vladimir Balabanov*, Bernard Grossman†, William H. Mason‡, and Raphael T. Haftka§

Multidisciplinary Analysis and Design (MAD) Center for Advanced Vehicles
Virginia Polytechnic Institute and State University
Blacksburg, Virginia 24061

An investigation of the aerodynamic modeling requirements for HSCT design has been made. Studies have been performed to determine the effects of including Euler/Navier-Stokes calculations for the supersonic aerodynamic performance and structural loading of HSCT designs. Accuracy, computational effort, and ease of implementation are some of the considerations which are addressed. We quantify the increase in accuracy of the CFD calculations over linear supersonic methods through comparison with experimental data. As expected, it was found that the Euler and parabolized Navier-Stokes solutions are more accurate than those from linear theory. For relatively thick bodies, significant increases in the accuracy of the zero-lift wave drag prediction can be obtained using CFD in place of slender body results. However for more slender bodies and wings like those for our HSCT designs, this improvement is drastically reduced. Investigation into the force and moment data for wings and wing-fuselages show several consistent patterns. For our HSCT wings, parabolized Navier-Stokes predictions on the viscous drag matched closely with those predicted from algebraic skin friction estimates. The linear supersonic theory results consistently overpredict the lift and underpredict the drag as compared to CFD. These drag differences have a large effect on the HSCT range calculations. Another significant difference between the CFD and linear supersonic theory results comes in the wing stresses calculated from the aerodynamic loads. The HSCT carries large amounts of fuel in its wings, and consequently has large inertia relief that cancels most of the bending moments due to aerodynamic loading. As a result, the wing bending stresses are very sensitive to the predicted location of the center of pressure. Relatively small differences in the predicted center of pressure location between Euler and linear theory resulted in significant differences in the wing bending stresses and the structural weights.

1. Introduction

Procedures for the combined aerodynamic-structural design optimization of a high-speed civil transport (HSCT) have been developed recently at Virginia Tech.[1–4] The detailed aerodynamic analyses in these studies involve what we term *linear supersonic theory*, comprising slender body results for wave drag, a linear theory panel code modified with leading-edge suction corrections for drag-due-to-lift and supersonic loads, and skin friction estimates. These analyses are used to predict, among other things, the drag at cruise as well as the supersonic loads for the structural optimization. The overall purpose of this paper is to investigate the implications of supplementing the linear supersonic theory calculations in our HSCT optimization with Euler and Navier-Stokes computations. To achieve this goal, we first validate and then certify an Euler/Navier-Stokes code for HSCT applications at both supersonic cruise and at off-design conditions. This paper will concentrate on the supersonic flight regime. The accuracy of the range estimates based on Euler and Navier-Stokes results are compared with those from the linear supersonic theory. We also compare the accuracy of the loads calculated by Euler/Navier-Stokes with linear supersonic theory and examine the effects of the differences of the results on the structural optimization.

Background

The HSCT design problem considered in Refs. 1–4 involves the minimization of the take-off gross weight (TOGW) with a range constraint of 5500 n.mi., a cruise Mach number of 2.4, and 251 passengers. The optimization uses 70 constraints which can be grouped into three categories: geometric constraints, performance/aerodynamic constraints, and constraints im-

*Graduate Research Assistant, Dept. of Aerospace and Ocean Engineering, Student Member AIAA

†Professor and Head, Dept. of Aerospace and Ocean Engineering, Associate Fellow AIAA

‡Professor of Aerospace and Ocean Engineering, Associate Fellow AIAA

§Professor of Aerospace Engineering, Mechanics and Engineering Science, University of Florida, Gainesville, FL, Associate Fellow AIAA

plicit in the analysis. The implicit constraints are a part of the analysis or geometry definition and are not handled directly by the optimization. They include an altitude limit, a fuselage volume constraint, and wing mean aerodynamic chord and nacelle orientation specifications. The wing shape, fuselage shape, tail areas, and nacelle sizes and locations are described using 26 design variables with two additional variables for the mission profile and another for the fuel, giving a total of 29 design variables. To efficiently perform the optimization, a variable-complexity modeling (VCM) technique (Refs. 1–4) has been employed. This technique utilizes both simple and complex models for predicting aerodynamic performance and structural weights. The simple conceptual-design-level methods are predominantly used in the optimization due to their very low computational costs. More accurate and more computationally expensive methods are used to periodically update the simpler models. In this way, one incorporates the accuracy of the higher level codes with the computational efficiency of the simpler models.

The linear supersonic theory used as our current detailed model includes the Harris[5] wave drag program, a panel method by Carlson[6] *et al.* with attainable leading-edge thrust corrections[7], and standard algebraic estimates of the skin friction using the Van Driest II method. In the present work, we are investigating the benefits of introducing Euler/ Navier-Stokes computations as the next level of complexity in the hierarchy of supersonic aerodynamic prediction models.

Related studies[8–11] on the use of CFD methods for supersonic HSCT design have appeared elsewhere. For pure analysis, Hollenback and Blom[8] compared PNS results with experimental data, Euler, and linear theory results for a Mach 2.4 HSCT design. Pittman[9] *et al.* obtained Euler equation solutions for a Mach 3 HSCT concept, and compared the results with linear theory. Their predictions were later verified by comparison to experimental data[10]. In each case, linear theory slightly overpredicted the lift, underpredicted the drag, and produced poor pitching moment results. However, Pittman[9] *et al.* concluded that linear theory was still useful in conceptual and preliminary design.

Mann and Carlson[11] evaluated the use of Euler analysis within the design context. Looking at pressure distributions, they proposed a method to overcome linear theory deficiencies and concluded that there was no significant advantage to the use of Euler codes in their wing design procedures.

Fluid Dynamics Code

We are using the General Aerodynamic Simulation Program[12] (GASP) version 2.2 for the Euler and parabolized Navier-Stokes (PNS) calculations. The PNS equations are a subset of the complete Navier-Stokes equations valid in supersonic conditions in which the streamwise shear stress terms are neglected. By suppressing a portion of the streamwise pressure gradient the equation type is changed from elliptic to parabolic, allowing the solution to be space marched in the streamwise direction. The PNS equations can predict crossflow separation but not streamwise separation. For our PNS calculations, the flow is considered to be fully turbulent, and the Baldwin-Lomax turbulence model is used. GASP is a fully conservative CFD code which solves the Reynolds-averaged Navier-Stokes equations and many of its subsets. The code uses an upwind three-dimensional finite-volume spatial discretization. Roe, Van Leer, Steger-Warming, and full flux functions are available in each direction. For our calculations, a fully upwind second order interpolation is used in the marching direction, and a third order upwind biased interpolation is used in the other two directions.

The finite-volume formulation of the Reynolds-averaged Navier-Stokes equations may be written in terms of the vector of conserved variables, Q, the vector of primitive variables, q, the cell volume, V, and a residual vector, $R(q)$, as

$$\frac{\partial <Q>}{\partial q}\frac{\partial <q>}{\partial t}V + R(q) = 0.$$

The cell average quantity, $<Q>$ is defined by integrating over the volume of the cell

$$<Q> = \frac{1}{V}\iiint_V Q(x,y,z,t)\,dV.$$

The residual vector can be written as a function of the inviscid fluxes, $\vec{F}$, the viscous fluxes, $\vec{F}_v$, the unit normal vector to the cell face, $\hat{n}$, and the area of the cell face, ΔA, as

$$R(q) = \sum_{j=1}^{nface}\left(\vec{F} - \vec{F}_v\right)\cdot\hat{n}\,\Delta A.$$

The norm of this residual vector represents the convergence to the steady state solution or the error in approximation of the discretized solution. GASP iteratively solves the system of equations until a prescribed tolerance on the norm of the residual is met. GASP can implement global iteration techniques as well as space-marching schemes for supersonic flows.

Due to the large savings in computational time, space-marching has been performed for all of the supersonic CFD calculations presented in this report.

CFD Grids

The grids for the space-marching calculations on HSCT wings and wing-fuselage combinations are created using a 3-D grid generator originally developed by Ray Barger at NASA Langley[13,14] and modified in the present work. The original grid generator has been modified to give better resolution of the wing leading-edge geometry. In addition, the code has been improved to be more robust for large planform variations. The grid generator receives as input the aircraft configuration stored in the Craidon[15] geometry format, extends the wing to join the fuselage, adds a fillet at the wing-fuselage intersection, and then creates a grid for a space marching calculation. Since our HSCT optimization code creates a Craidon description file from its set of design variables, the conversion from a set of design variables to a space marching grid is straightforward. The outer boundary is calculated from a Mach cone analysis to ensure that all shocks are contained within the computational domain. The grid generator allows for flexible stretching of the grid points around and normal to the aircraft for use in grids suitable for both Euler and Navier-Stokes calculations. Measures are employed to reduce grid skewness at the wing tip and wing-fuselage juncture. The grid generator is automated and robust for large planform changes. These qualities are required for design optimization applications.

Structural Optimization

The structural analyses and optimization are performed using the general purpose finite-element (FE) structural optimization code GENESIS.[16] The FE model used in the structural analysis consists of 451 rods, 383 membrane elements, and 129 shear panels. The 963 elements are joined together at 193 nodes with a total of 1032 degrees of freedom. Optimizations can be performed using the method of Feasible Directions, Sequential Linear Programming method, and Sequential Quadratic Programming method. We use Method of Feasible Directions for our problem. A coarse-grain parallel version of GENESIS has been implemented on the Intel Paragon computer at Virginia Tech (Ref. 17). This is a 28 node parallel computer with distributed memory. An automated structural mesh generator[18] has been developed to construct the FE model for the HSCT configuration. As with the space-marching CFD grid generator, the FE grid generator uses the Craidon description of the aircraft.

Code Verification and Certification

As CFD technology matured, code verification became important. In 1988, Bobbitt[20] presented a comprehensive survey of code verification issues, and AGARD held a conference[19] on verification of CFD codes. Since then, the establishment of a rigorous basis for verifying and certifying codes has been found to be more difficult than originally envisioned. An excellent discussion has been given by Aeschliman[21] *et al.*

To assess the usefulness of including CFD results in the variable complexity modeling approach to HSCT optimization, the guidelines on code certification procedures outlined by NASA and the Multidisciplinary Analysis and Design Industrial Consortium (MADIC)[22-24] have been followed. First in this process is the code *verification*, which establishes an acceptable level of accuracy in the calculation. The MADIC/NASA panel defines verification as "the process that demonstrates the code's ability to solve the specific set of governing equations and boundary conditions posed to the computer by the code."[23] Grid refinement studies and comparison to experimental data are key components in this process. The *validation* step then ensures that the code properly models the flow physics. The *certification* of the code for the specific design applications can take place only after these steps are completed. Certification assesses the adequacy of the code for a specific class of applications. For optimization, the key issues are accuracy, robustness, computational effort, and ease of implementation. The trade-off between accuracy and computational effort is of practical significance.

Outline

We begin to address these issues by comparing the wave drag predictions from the Harris code and those from CFD calculations with experimental data on simple analytic axisymmetric forebodies and on symmetric wings. Grid and residual convergence studies are performed to give insight into the mesh sizes and computational effort required to achieve converged results. Next, we compare the integrated forces and moments for wings and wing-body combinations predicted from the linear supersonic theory and CFD. The impact of the differences in the forces on the HSCT range calculation is then investigated. After looking at the effects of the integrated forces on the HSCT performance, the focus shifts

to the effects of the distributed loads on the structural analysis. The stresses calculated using loads determined from linear supersonic theory and from CFD are compared at the cruise condition and for other load cases. These loads are then used in the structural optimization to compare the wing bending material weights computed using linear supersonic theory loads and CFD loads. From these investigations we attempt to determine when in the design optimization process it is advantageous to move from linear supersonic theory to higher level CFD analyses.

2. Code Verification

Haack-Adams Bodies

Our studies begin by investigating the zero-lift wave drag prediction for a series of Haack-Adams bodies.[25] Calculations have been performed using two different fineness ratios: $l/d_{max} = 7$ and $l/d_{max} = 10$. The equation for the radius, r, of these bodies with area ratio $A_{base}/A_{max} = 0.532$ is given as:

$$\begin{aligned}\frac{r}{r_{max}} &= \left\{0.707\left[1-\left(\frac{2x}{l}-1\right)^2\right]^{3/2}\right. \\ &+ 0.16934\left(\frac{2x}{l}-1\right)\left[1-\left(\frac{2x}{l}-1\right)^2\right]^{1/2} \\ &+ \left.0.16934\cos^{-1}\left(1-\frac{2x}{l}\right)\right\}^{1/2}.\end{aligned}$$

Investigation of the body shape (Fig. 1) reveals that the nose is blunt. This limits the grid resolution of the nose to densities that allow a space marching solution. However, following work by Mason and Lee,[26] the CFD solutions were space marched as if the nose was sharp. They showed that the bluntness is so small for this minimum drag shape that explicitly including a blunt nose computation does not change the drag.

The convergence study of the wave drag with mesh size (Fig. 2) for the Euler equations was performed for the body with $l/d_{max} = 10$ at Mach 2.5. An axisymmetric grid was used for these calculations, so the total number of cells, N, is the number of axial cells times the number of normal cells. Meshes with uniform axial spacing and with distributions clustered at the nose are considered. For the clustered grids, two different grid aspect ratios are considered. One has an equal number of axial and normal points, while the other has twice the number of axial points as normal points. The clustered grids with a $1:1$ (*normal:axial*) grid ratio range in size from 11×11 to 71×71. The clustered grids with a $1:2$ grid ratio range in size from 11×21 to 41×81. The uniform grids with a $1:2$ grid ratio range in size from 11×21 to 81×161.

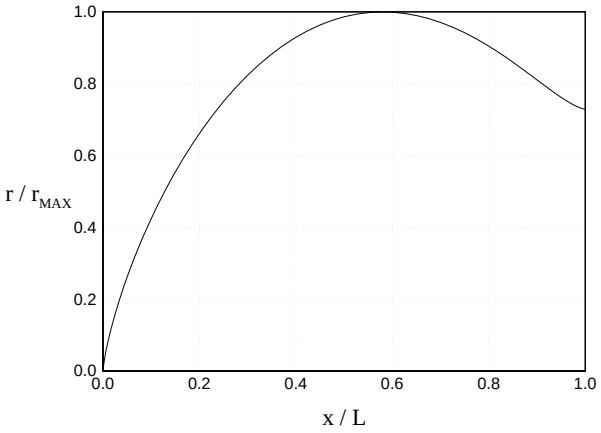

Figure 1: Haack-Adams Body Shape

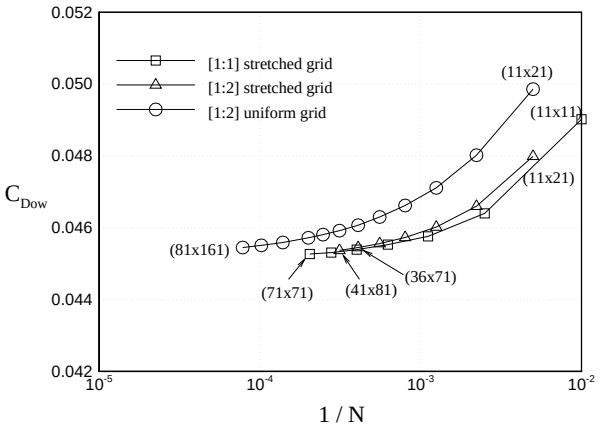

Figure 2: Haack-Adams Grid Convergence

Clearly, the grids with axial points clustered near the nose outperform the grids with uniform axial spacing. Both the 36×71 and 51×51 clustered grids produce converged results, where our criteria for convergence is computed drag values within one percent of the extrapolated value as $N \to \infty$. Since the 36×71 grid has 50 fewer grid cells than the 51×51 grid, it was chosen for use in the Euler computations. The drag for these bodies is non-dimensionalized using the freestream conditions and the maximum cross-sectional area, A_{max} of the body.

Convergence with residual (Fig. 3) is investigated on the clustered 71×71 grid. Converging the resid-

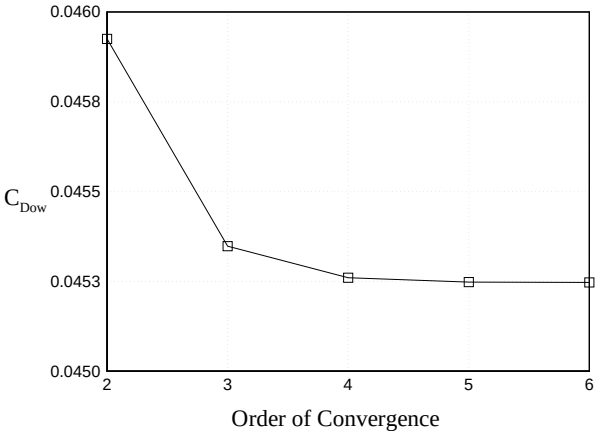

Figure 3: Haack-Adams Residual Convergence

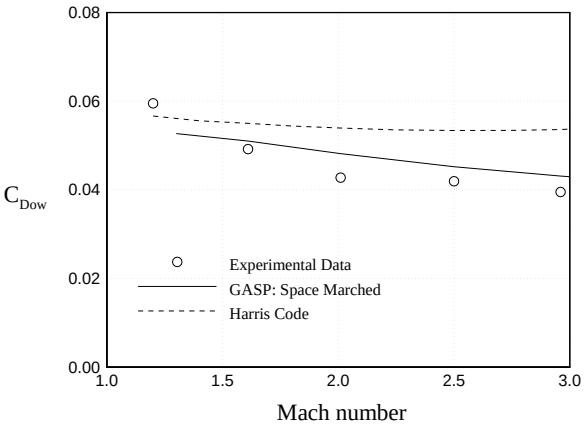

Figure 5: Haack-Adams Body $l/d_{max} = 10$

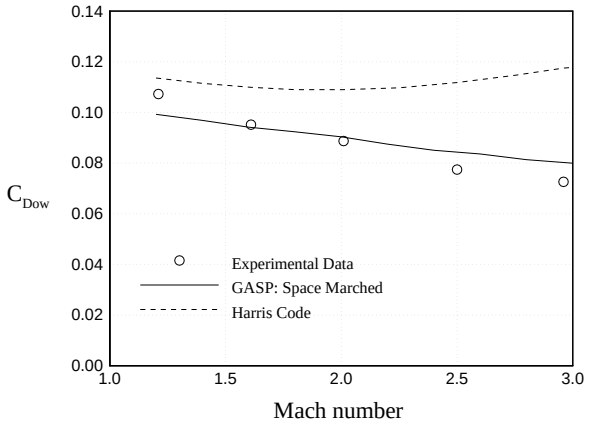

Figure 4: Haack-Adams Body $l/d_{max} = 7$

ual four orders of magnitude results in a wave drag prediction within 0.0001 of the extrapolated value. The *order of convergence* plotted in the graph refers to how many orders of magnitude the residual is reduced from its value at the first iteration. Mathematically it can be written as

$$\text{order of convergence} = -log_{10} \frac{||R||^{(i)}}{||R||^{(1)}}$$

where $||R||^{(i)}$ is the norm of the residual vector at the i^{th} iteration. All other calculations on the Haack-Adams body are performed with this convergence criterion.

The Euler wave drag predictions show substantial improvement over the Harris wave drag code results (Figs. 4,5) for both the $l/d_{max} = 7$ and $l/d_{max} = 10$ cases. The Harris code performs poorly with increasing Mach number for this case. While the experimental data and Euler prediction of the wave drag decrease with Mach number, the Harris code wave drag prediction begins to increase with Mach number. As expected, the accuracy of the Harris wave drag results does improve for the more slender body.

The computational time required for the Euler analysis of the Haack-Adams forebody is approximately three minutes (0.07 sec/cell) for the clustered 36×71 grid on a single processor SGI R4000 workstation. By comparison, the Harris wave drag code takes less than one second to compute the drag.

Squire Wing

We now investigate the wave drag prediction on a symmetric delta-wing. The Squire Wing (Fig. 6) is a delta wing with a biconvex centerline and elliptic cross-section. The thickness of each cross-section is chosen to match the cross-sectional area of a 9% thick biconvex wing with a diamond-shaped cross-section[27]. The space marching grid is created with the grid points clustered near the wing in the same way they were for the Haack-Adams body. The wing surface grid is also clustered along the leading edge to properly define the elliptical cross-section geometry.

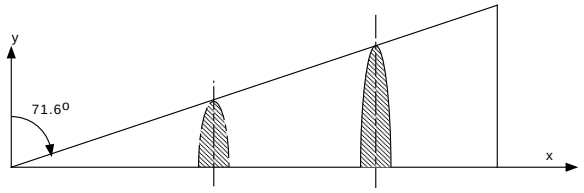

Figure 6: Squire Wing

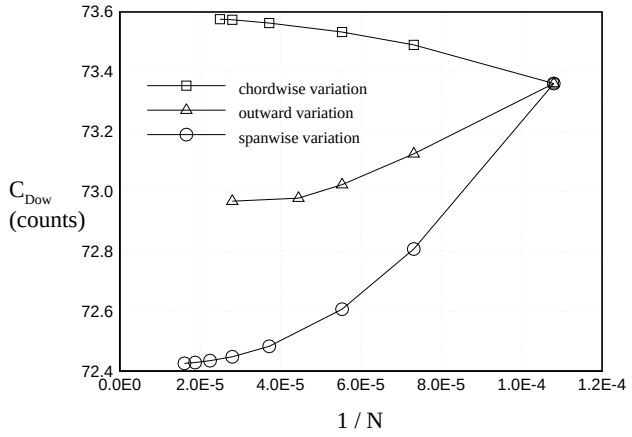

Figure 7: Grid Convergence for Squire Wing

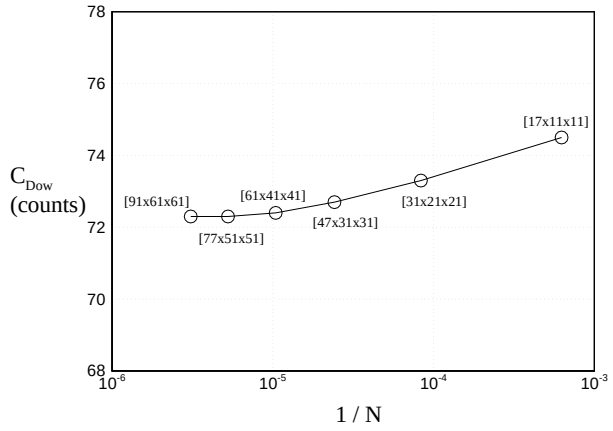

Figure 8: Grid Convergence for Squire Wing

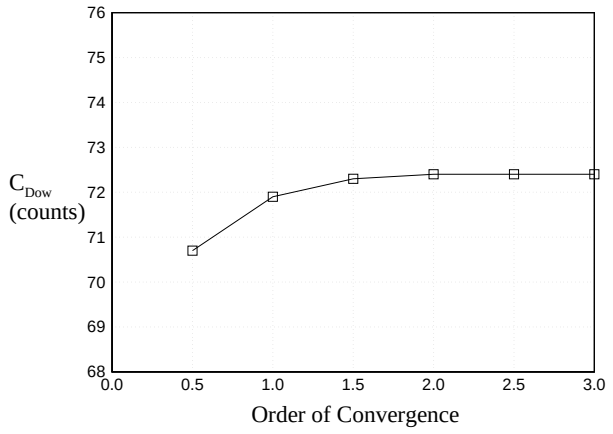

Figure 9: Residual Convergence for Squire Wing

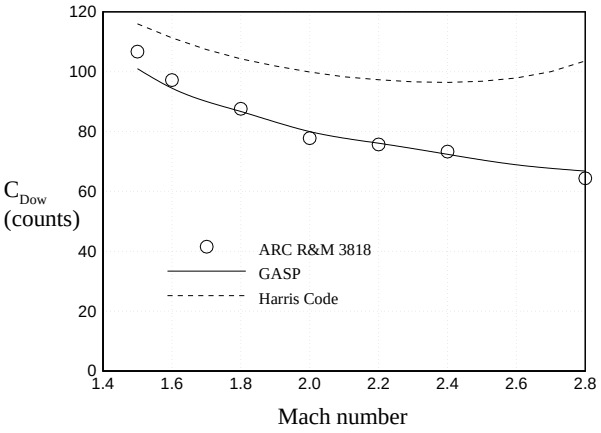

Figure 10: Squire Wing Wave Drag

Grid refinement studies are performed on the wing at 0° angle of attack and Mach 2.4. Figure 7 shows the relative effects of varying the number of grid points in only one direction. This is done to identify the dimension to which the wave drag is most sensitive. The drag coefficient data, based on the planform area, is given in *counts* of drag, where one count of drag is equivalent to $C_D = 0.0001$. The coarsest grid considered is 21×21×21. The number of spanwise, outward, and chordwise points are increased to 141, 81, and 101 respectively. As expected, the number of spanwise points is found to have the largest effect on the drag. Note that the scale for this graph is very small. The total change in drag from the coarsest to finest grid for the spanwise variation is slightly less than one count. With this in mind, a grid convergence study (Fig. 8) for a [3:2:2] aspect ratio grid [*spanwise*:*outward*:*chordwise*] is investigated. The 61×41×41 grid was chosen for our computations since it gives results within one percent of the extrapolated mesh value as $N \rightarrow \infty$. The residual convergence study (Fig. 9) performed on the 61×41×41 grid at Mach 2.4 indicates that converging the solution two orders of magnitude is sufficient. This is less stringent than the Haack-Adams result.

Inspection of the wave drag results (Fig. 10) shows good agreement between GASP and the experimental data. The Harris wave drag results show the same overprediction found in the results for the thickest Haack-Adams body. The Euler computation for the 61×41×41 grid took about 19 minutes (0.012 sec/cell) on an SGI R4000 workstation.

High-Lift Maneuver Wing

The study will now focus on the force and moment predictions from our linear supersonic theory and from GASP. A high-lift maneuver wing[29–31] with experimental force and moment data and pressure distributions was selected to assess the accuracy of the codes. The high-lift wing (Fig. 11) is only slightly cambered in the streamwise sections, but there is pronounced spanwise cambering. Another feature of this wing is that, due to its design, inviscid flow conditions predominate on the upper surface.

The wing was tested at Mach 1.62 and angles of attack ranging from 0° through 14°. The Euler calculations are performed with a 77×51×77 grid (*spanwise*×*outward*×*chordwise*). This grid was chosen following a convergence study in Section 3. Calculations on this grid took about 18 minutes (0.004 sec/cell) on an SGI Power Challenge XL. A 77×91×77 grid was chosen for the PNS calculations from the grid convergence study in Figure 12. The PNS grid contains approximately 40 grid cells in the boundary layer (Fig. 13) with the first cell well inside the laminar sublayer ($y^+ \approx 1.0$). Computations on this grid took about 2.5 hours (0.017 sec/cell) on an SGI Power Challenge XL to converge. All PNS computations were performed on the Power Challenge XL, which is 4–5 times faster than the SGI R4000 workstation previously mentioned. Grid converged results were therefore obtained with meshes having the same number of cells in the inviscid region for both the PNS and Euler grids. Converging the residual two orders of magnitude was found to be sufficient for both the parabolized Navier-Stokes and Euler computations on this wing. The results from the Euler and linear theory codes are adjusted to include an

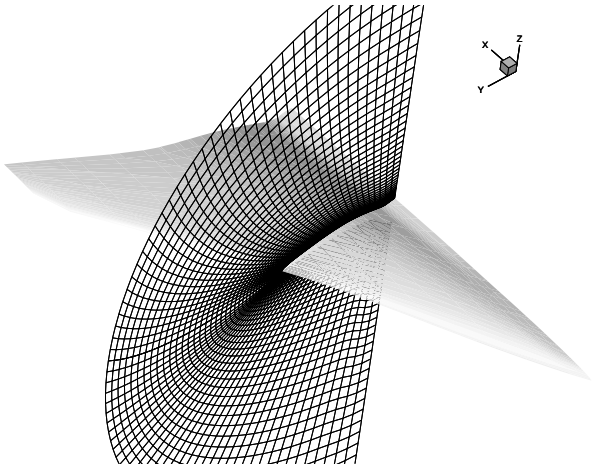

Figure 11: Supersonic Maneuver Wing

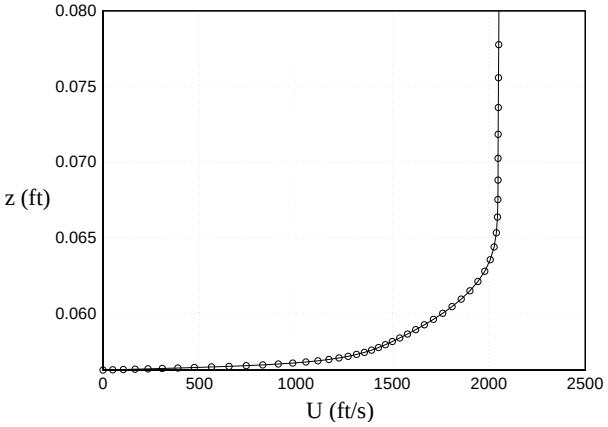

Figure 13: Boundary Layer Profile

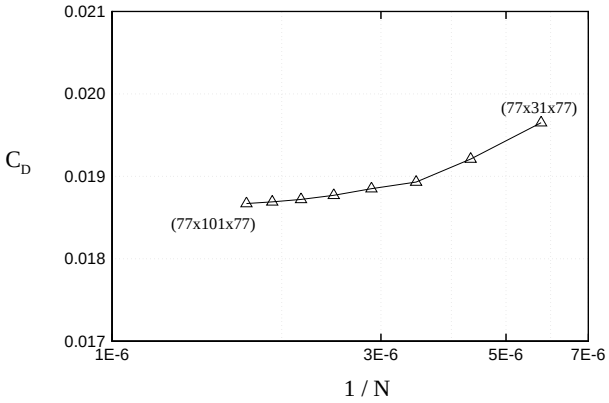

Figure 12: PNS Grid Convergence Study

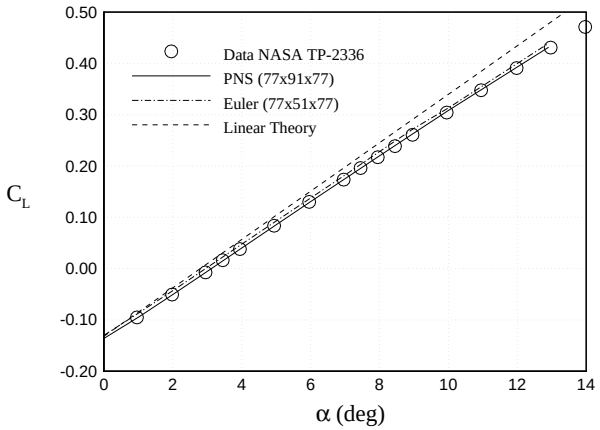

Figure 14: Lift Coefficient for Maneuver Wing

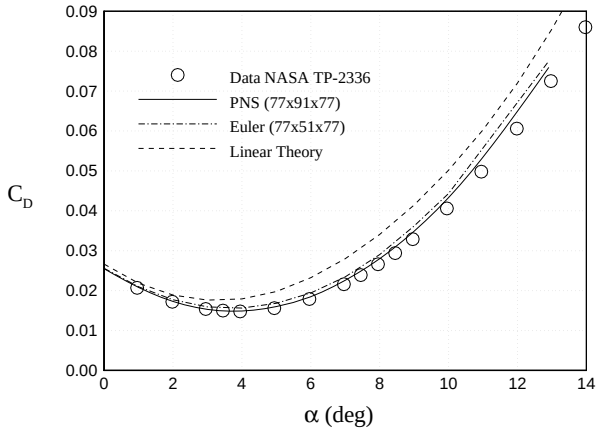

Figure 15: Drag Coefficient on Maneuver Wing

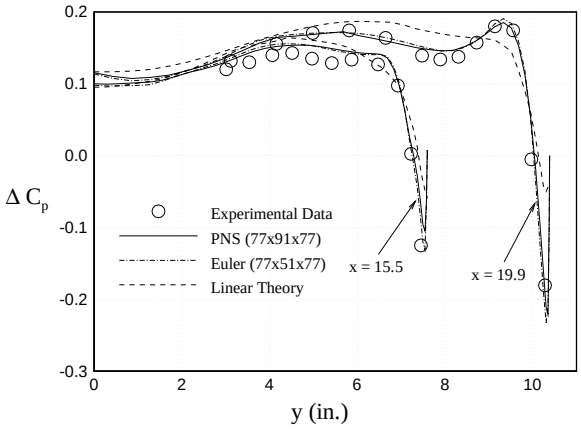

Figure 17: Load Distributions at $\alpha = 5.98°$

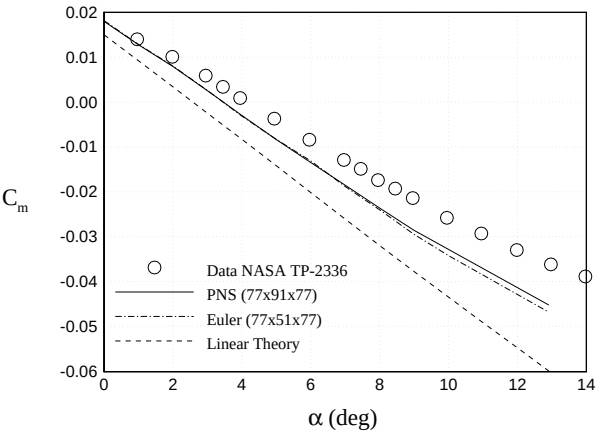

Figure 16: Pitching Moment Coefficient for Maneuver Wing

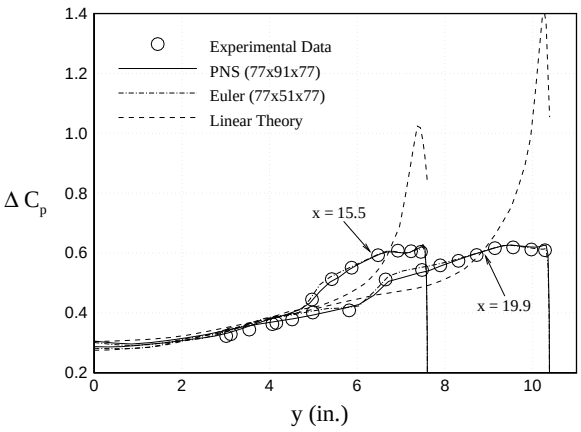

Figure 18: Load Distributions at $\alpha = 12.91°$

axial friction drag coefficient of 0.0069 to compare with the experimental data. This viscous correction was obtained by Pittman[31] *et al.* using the method in Ref. 32. This viscous term is assumed to be invariant with the angle of attack. The CFD results compare well with the experimental data (Figs. 14–16).

The PNS results show slightly better agreement than do the Euler, but both outperform the linear theory results, especially at the larger angles of attack. There is a 7.5% overprediction in the linear theory lift-curve slope, C_{L_α}. The panel code drag prediction deteriorates with increasing angle of attack. The pitching moment is taken about the point $x = 16.701, y = 0.0, z = -0.275$, where the origin of the coordinate system is the wing apex. The pitching moment shows the greatest discrepancy. The Euler and PNS pitching moment results are significantly more accurate than the panel code results, but still differ from the experimental data.

The load distributions (Fig. 17) for this wing at 5.98° show the CFD results matching well with experimental data. The distributions computed from linear theory give the correct general shape, but do not capture the details as well. This is evident in the $x = 19.9$ curve where the peak and drop in ΔC_p near the leading edge are completely smoothed out.

The load distributions (Fig. 18) for the same wing at 12.91° angle of attack show a much more dramatic picture. Again the CFD results do an excellent job predicting the load distribution. This wing has a crossflow shock at this condition, which is captured by the CFD analyses. However, the panel code results are much worse than those for the lower angle of attack cases. In particular, the leading-edge sin-

gularity predicted by linear theory does not appear in the data or nonlinear calculations.

3. Code Certification

HSCT Fuselage

Now that we have established a level of confidence in the CFD results, we begin investigations into the prediction of forces, moments, and loads for our HSCT designs. An axisymmetric HSCT body is considered first. We create the fuselage for our HSCT configurations with 8 design variables that define the axial location and radius of the fuselage at four positions. The shape of the body between these points is then determined by considering it as a minimum wave drag body of a fixed volume[1,33]. The cross-sectional area is given by

$$\begin{aligned} S(\tilde{x}) &= \frac{128V}{3\pi l}\tilde{x}^{3/2}(1-\tilde{x})^{3/2} \\ &+ l^2\sum_{i=1}^{4}\nu_i\Big[\ln\left(\frac{z_{1i}+2z_{2i}}{z_{1i}-2z_{2i}}\right) \\ &+ \frac{2z_{2i}}{9}\left(9z_{1i}-64z_{2i}^2\right)\Big], \end{aligned}$$

where $z_{1i} = \tilde{x}+k_i-2\tilde{x}k_i$ and $z_{2i}^2 = \tilde{x}k_i(1-\tilde{x})(1-k_i)$. The quantity V is the fixed volume, l is the fuselage length, $\tilde{x}$ is the normalized axial location x/l, and the k_i are the normalized axial locations of the restraints. The constants ν_i are determined by solving the 4×4 linear system resulting from this equation applied at the four restraint locations. A typical fuselage shape is shown in Figure 19. The plot shows the reduced area in the fuselage mid-section, which gives improved area ruling of the wing-fuselage designs. This fuselage does not have the bluntness of the Haack-Adams forebody.

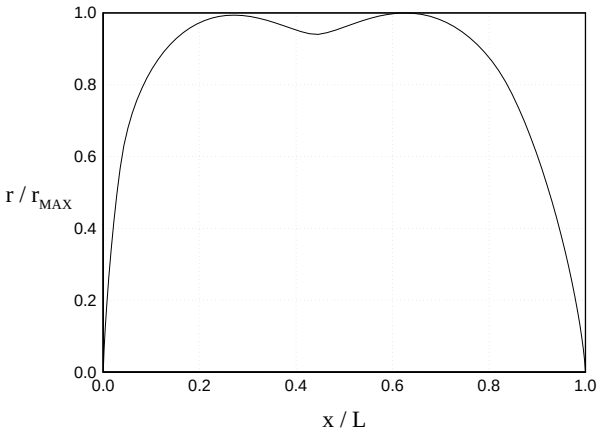

Figure 19: HSCT Fuselage

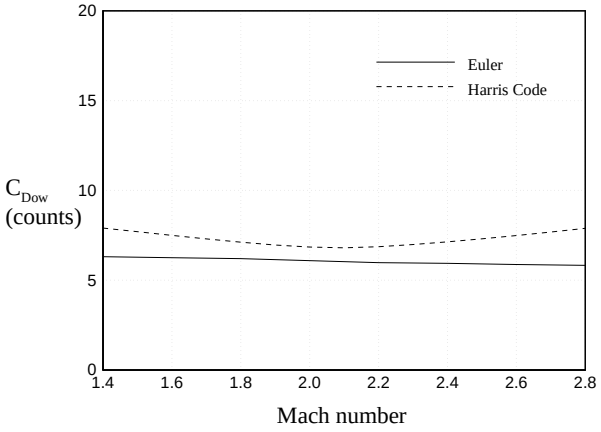

Figure 20: HSCT Fuselage Wave Drag

In contrast to the Haack-Adams bodies, which had fineness ratios of 7 and 10, the more slender HSCT fuselages have $l/d_{max} = 25$. As a result, the differences between the Harris code and Euler predicted wave drag (Fig. 20), present in the Haack-Adams body results, are much smaller. In this case, the drag is non-dimensionalized using the freestream conditions and the area of the wing corresponding to this fuselage. The minimum difference between the Euler calculations on a 41×81 (*normal*×*axial*) grid and Harris wave drag is approximately 0.8 counts of drag near Mach 2.0. The maximum difference in the Euler and Harris code prediction of the wave drag over this Mach number range is 2.0 counts.

Uncambered HSCT Wing

The first HSCT cranked wing studied is an uncambered wing with no trailing-edge sweep. This was chosen to ensure that the trailing edge of the wing would be accurately modeled by the space marching grid, which is created using $x = constant$ marching planes. The design variables used to describe this wing are given in Table 1. These wing parameters are described in detail in Ref. 2.

Figure 21 shows the wing-body along with slices of the Euler marching grid. The wing-alone grid was created from the wing-fuselage design by removing the fuselage and extending the wing to the centerline. Grid refinement studies (Fig. 22) for the Euler computation were performed for this wing at 4° angle of attack in a Mach 2.4 flow. Three grid aspect ratios (*spanwise:outward:chordwise*) were considered: [1:1:1], [3:2:2], and [3:2:3]. For the [1:1:1] aspect ratio, the coarsest grid considered is 11×11×11 and the finest is 51×51×51. For the [3:2:2] aspect ra-

Table 1: Variables for Wing Definition

	Value	Description
1	181.00	Wing Root Chord (ft.)
2	156.00	L.E. Break, x (ft.)
3	49.20	L.E. Break, y (ft.)
4	181.00	T.E. Break, x (ft.)
5	64.00	T.E. Break, y (ft.)
6	170.00	L.E. Wing Tip, x (ft.)
7	11.00	Wing Tip Chord (ft.)
8	75.90	Wing Semi-Span (ft.)
9	0.4019	x-Loc. Airfoil Max. t/c (x/c)
10	3.6921	L.E. Radius Parameter
11	2.5789	t/c at Wing Root (%c)
12	2.1594	t/c at L.E. Break (%c)
13	1.8039	t/c at Wing Tip (%c)

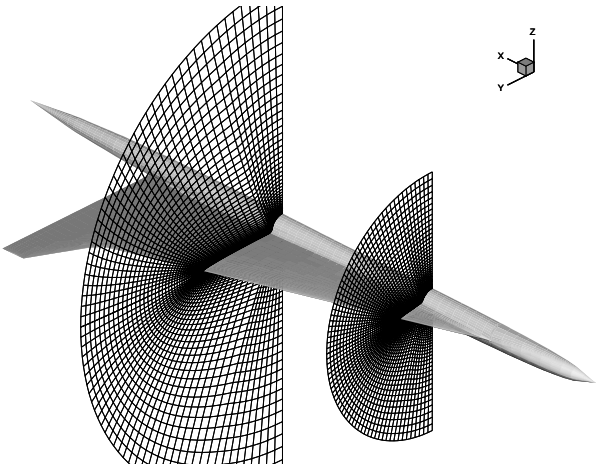

Figure 21: HSCT Wing-Fuselage and Grid Slice

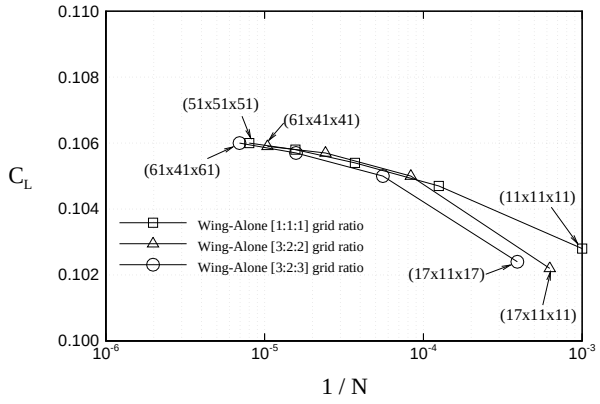

Figure 22: Lift Convergence with Grid

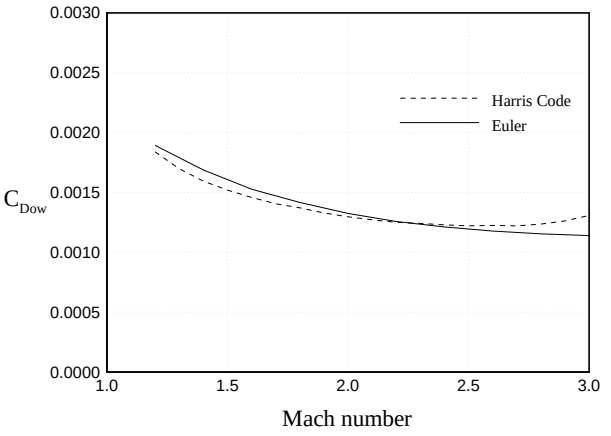

Figure 23: Wave Drag Prediction for HSCT Wing

tio, the coarsest grid is 17×11×11 and the finest is 61×41×41. Finally, for the [3:2:3] aspect ratio, the coarsest grid investigated is 17×11×17 and the finest is 61×41×61. The small scale for the range of the convergence plot should be noted. The study shows that the [3:2:2] ratio grids give comparable results to the other aspect ratio grids with fewer total grid cells. The 61×41×41 grid gives converged results with the fewest number of grid cells, and is therefore used for all Euler computations on this wing. Following the grid convergence study (Sect. 2) for the high-lift maneuver wing, a 77×91×77 grid was used for the PNS calculations

The comparison between the Harris code and Euler predictions for the volumetric wave drag are presented in Figure 23 As expected, the results for the zero-lift wave drag on this nominally 2.5% thick wing show much closer agreement than those for the 9.0% thick Squire wing. Euler calculations and Harris code predictions of the zero-lift wave drag match within 1.5 counts for Mach numbers ranging from 1.2 through 3.0.

When the integrated force and moment data were analyzed, many of the same trends that were present in the maneuver wing were seen again. Linear supersonic theory results show a 4.2 percent overprediction of the lift curve slope (Fig. 24). The algebraic skin friction estimate predicted a viscous drag coefficient of 0.00266. This agrees well with the PNS calculations which give a nearly constant viscous drag coefficient around 0.00251. Figure 25 shows the good agreement between the PNS drag and Euler drag prediction with algebraic skin friction corrections. The linear supersonic theory drag with viscous corrections compares well to Euler and PNS at

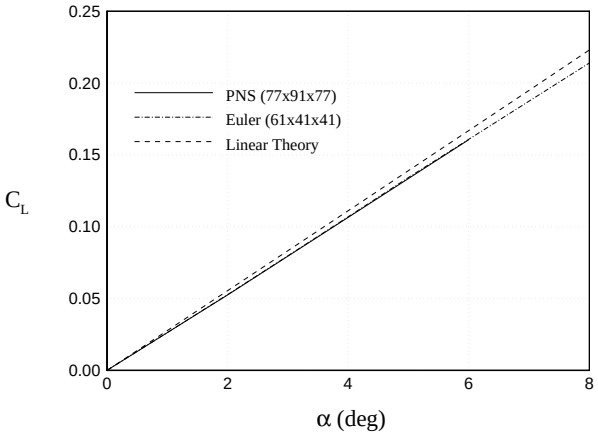

Figure 24: Lift Coefficient for HSCT Wing

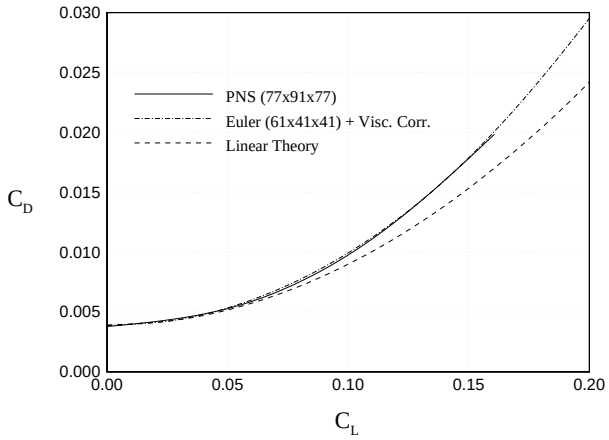

Figure 25: Drag Polar for HSCT Wing

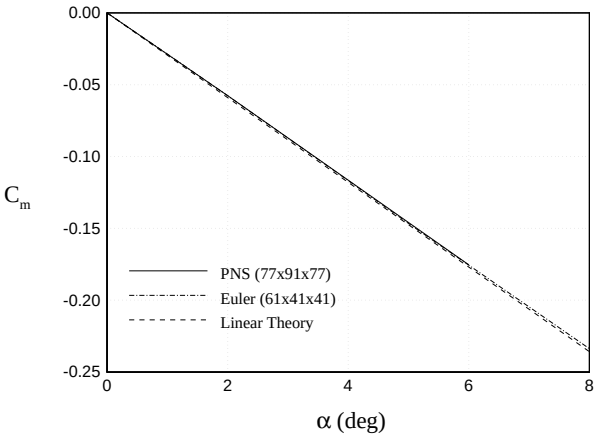

Figure 26: Pitching Moment Coefficient for HSCT Wing

lower lift values, but diverges as the C_L increases. At a typical cruise condition ($C_L = 0.08$), the linear theory drag prediction is 8 counts lower than the PNS prediction. For this wing, the pitching moment predictions (Fig. 26) from linear theory agree with our CFD results. For our HSCT wings, the pitching moment is taken about the wing apex.

The effect of the difference in drag predictions between linear theory and CFD on HSCT performance was assessed for this wing. For our baseline HSCT, the increase in range resulting from an 8 count underprediction in the drag predicted from linear theory was 600 n.mi. This corresponds to a sensitivity of 75 n.mi. per drag count. This is an analysis result. We have not (yet) performed an optimization using CFD aerodynamics.

The PNS computation takes close to 3 hours (0.021 sec/cell) on the SGI Power Challenge XL. On the same machine, the Euler calculation takes approximately 7 minutes (0.004 sec/cell), while the linear supersonic theory results take one second.

Cambered HSCT Wings

An aft-swept trailing-edge wing (Fig. 27) with a camber distribution found using the linear theory code WINGDES[34] is considered next. The design variables for this wing are given in Table 2. The sweep of the trailing edge is significant since the grid generator creates the marching planes at $x = constant$ locations. This results in a *stair-step* definition of the wing trailing edge. Grid refinement studies revealed that due to this trailing edge sweep, a denser mesh than was used for the previous wing was required to give converged results. A 77×51×77 grid is used for all calculations on this wing. As for the previous studies, a 77×91×77 grid is used for the PNS calculations.

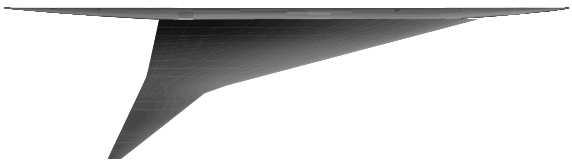

Figure 27: HSCT Wing-Fuselage

Table 2: Variables for Wing Definition

	Value	Description
1	169.47	Wing Root Chord (ft.)
2	143.34	L.E. Break, x (ft.)
3	37.73	L.E. Break, y (ft.)
4	176.05	T.E. Break, x (ft.)
5	30.39	T.E. Break, y (ft.)
6	189.83	L.E. Wing Tip, x (ft.)
7	7.02	Wing Tip Chord (ft.)
8	74.33	Wing Semi-Span (ft.)
9	0.4800	x-Loc. Airfoil Max. t/c (x/c)
10	3.2000	L.E. Radius Parameter
11	2.1400	t/c at Wing Root (%c)
12	1.7300	t/c at L.E. Break (%c)
13	1.5100	t/c at Wing Tip (%c)

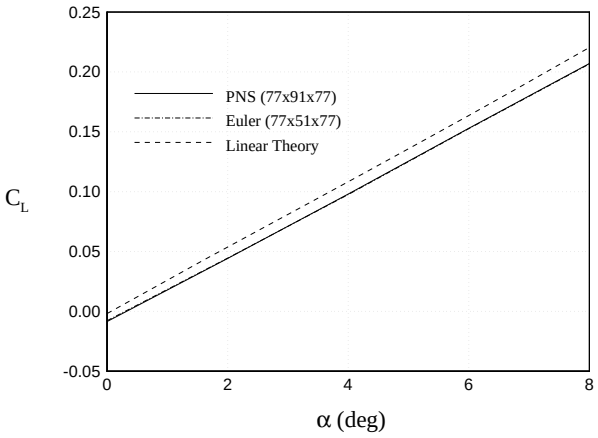

Figure 28: Lift Coefficient for HSCT Wing

The same trends in the force and moment data found previously are seen for this wing (Figs. 28–30). There is a 3.1% overprediction in C_{L_α} and a 5.0% underprediction in C_{m_α}, but there is also a discrepancy in the forces and moments at zero angle of attack that was not present for the uncambered wing. The algebraic skin friction estimate predicts a friction drag coefficient of 0.00248. This is within 2 counts of the viscous drag predicted from the PNS calculations. As with the previous wing, the drag polar shows good agreement between the PNS drag predictions and the Euler drag predictions with the viscous correction. In addition, we see the same deterioration in the linear supersonic theory drag as the lift increases. At the cruise C_L of 0.08, the difference between the PNS drag and the linear supersonic theory drag is 10 counts.

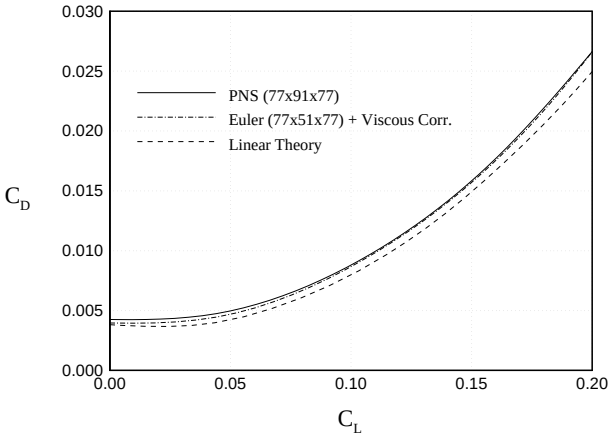

Figure 29: Drag Polar for HSCT Wing

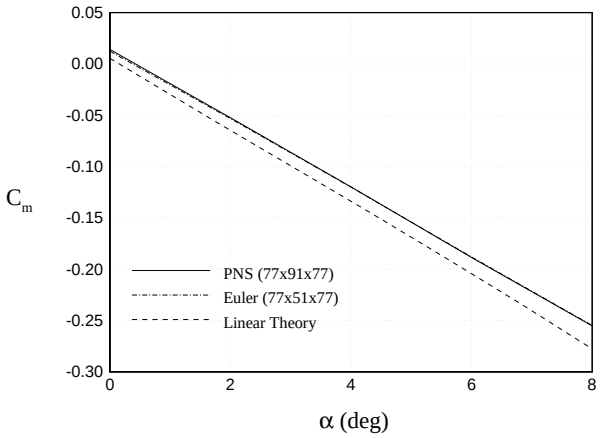

Figure 30: Pitching Moment Coefficient for HSCT Wing

The Euler computations took approximately fifteen minutes (0.003 sec/cell) while the PNS calculations took nearly three hours (0.021 sec/cell) to converge on the SGI Power Challenge XL. The increase in the computational cost per cell for the PNS calculations is mainly due to the smaller time step required to converge the solution.

HSCT Wing-Fuselage

In the next step, the forces and moments predicted by linear theory and Euler analysis for an HSCT wing-fuselage design are compared. The fuselage and uncambered wing from the previous wing-alone study are considered. Grid refinement (Fig. 31) suggests that a 77×51×77 grid is sufficient for the force and moment prediction. The grid refinement was run using the wing-fuselage design at 4° angle

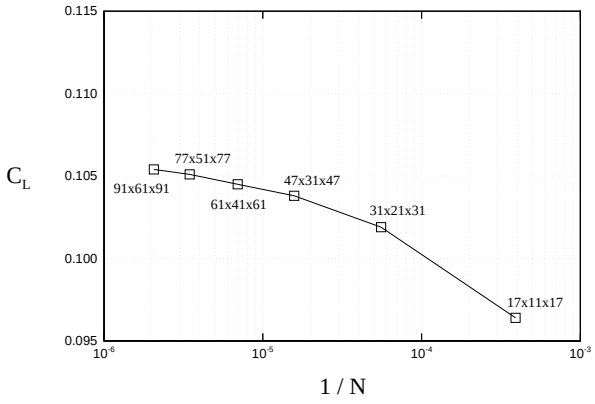

Figure 31: Lift Convergence with Grid

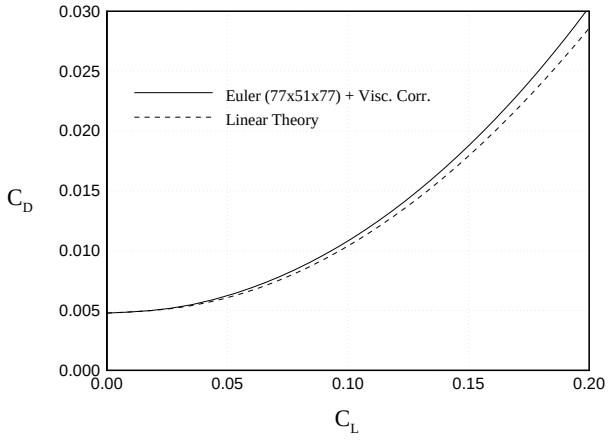

Figure 33: Drag Polar

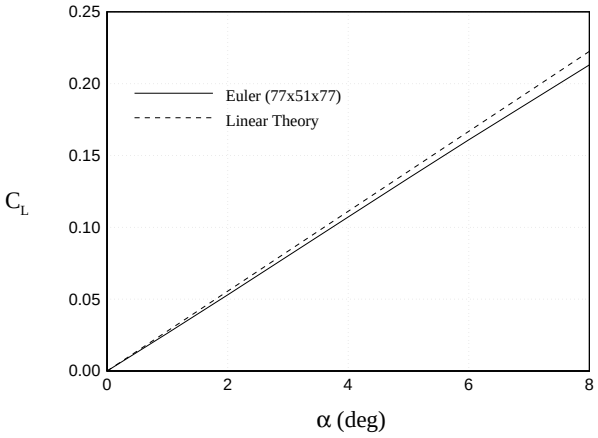

Figure 32: Lift Coefficient

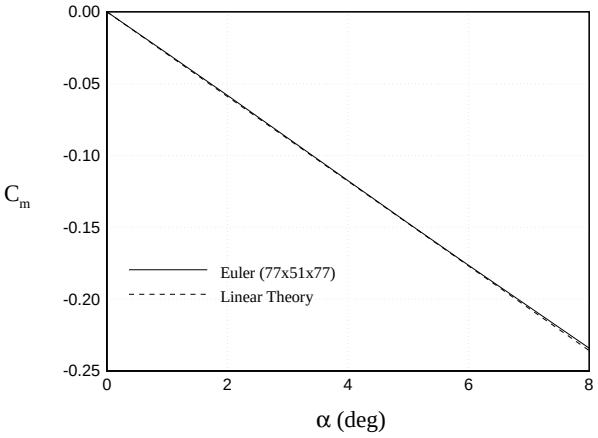

Figure 34: Pitching Moment Coefficient

of attack at Mach 2.4. The force and moment predictions (Figs. 32–34) for the Euler and linear supersonic theory show the same trends as the wing-alone case. There is a 4.2% overprediction in the linear theory prediction of C_{L_α} compared to Euler calculations. At $C_L = 0.08$, the linear theory drag prediction is 7.5 counts lower than the Euler prediction with the same algebraic friction drag of 0.00327 added. PNS calculations were not done for this case. The pitching moment computed from linear theory and the Euler equations again compare well.

The Euler code takes approximately forty minutes (0.008 sec/cell) to compute a solution at $\alpha = 0°$ on the SGI R4000 SGI machine. This time increased to about an hour (0.015 sec/cell) for non-zero angles of attack. The linear theory predictions again only take about one second.

Loads and Structural Optimization

We now turn our attention to the distributed loads used for the HSCT structural optimization. In a multidisciplinary design optimization, the constraints for the structural optimization are evaluated at a number of load cases. In Ref. 18, load cases including transonic climb, low-speed pull-up, and high-speed pull-up are considered. Some of these load conditions will now be examined using the cambered HSCT wing with aft swept trailing edge previously used in the wing study. The structure is assumed to be rigid for the determination of aerodynamic forces. Previous studies indicated that structural flexibility did not have a large effect on the loads for our HSCT configurations (Ref. 18). The three load cases considered in this report are a Mach 2.4 cruise, a Mach 1.2 cruise, and a 2.5g pull-up at Mach 2.4. The stresses in the wing were computed from the loads

Table 3: Center of Pressure Predictions

	Predicted y-Location of Center of Pressure ($ft.$)	
Load Case	Linear Theory	Euler
Mach 2.4 Cruise	26.55	24.88
Mach 1.2 Cruise	31.88	30.43
Mach 2.4 2.5g pull-up	29.13	27.31

predicted by both linear theory and the Euler equations. The computed wing bending stresses show significant discrepancies between the two cases. There is a $15\% - 20\%$ difference in the stresses computed from the Euler loads and those from linear theory loads for each of the three load cases. It was surprising that the Mach 2.4 cruise condition had compared so poorly for a small value of the lift coefficient of about 0.08.

The search for the cause of the stress differences led to investigations into the center of pressure predictions. For all of the load cases run on this wing, the spanwise location of the center of pressure predicted from linear supersonic theory and Euler had significant differences (Table 3). We see from the table that the Mach 2.4 cruise condition actually had one of the largest differences in predicted center of pressure locations of $1.67ft$. When a simple beam stress analysis was performed, it was found that the difference in spanwise location of the center of pressure accounted for a large portion of the difference in predicted stresses. Structural optimizations were also performed using the linear theory and Euler loads. The ratio of the wing bending material weights computed in the structural optimization from Euler loads and from linear theory loads was 0.875. A lighter wing was obtained using the Euler loads since the center of pressure was located inboard of the value predicted by linear theory.

A structural analysis was performed on another HSCT wing to test our conclusion about the importance of the center of pressure prediction. This wing (Fig. 35) has an unusual forward swept trailing edge. The difference in stresses predicted by linear theory and Euler are much lower for this wing. The Mach 2.4 cruise showed a $1-5\%$ difference in stresses, and the other two load cases had slightly larger $5-10\%$ discrepancies. As expected, the center of pressure predictions (Table 4) for this wing were much closer than they were for the previous wing. The largest difference between the Euler and linear theory predictions of the center of pressure location is only $0.35ft$. This difference occurs for the Mach 1.2 cruise condition. The ratio of wing bending material weights resulting from the structural optimization was also much closer to unity for this wing (1.015). Due to the large amounts of fuel in the HSCT wing, there is a large amount of inertial relief which cancels much of the bending due to aerodynamic loading. As a result, the bending stresses in the HSCT wing are sensitive to small differences in the predicted center of pressure location.

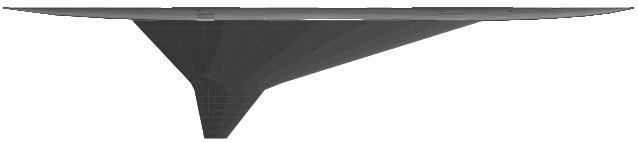

Figure 35: HSCT Wing-Fuselage

Table 4: Center of Pressure Predictions

	Predicted y-Location of Center of Pressure ($ft.$)	
Load Case	Linear Theory	Euler
Mach 2.4 Cruise	23.92	23.75
Mach 1.2 Cruise	26.35	26.01
Mach 2.4 2.5g pull-up	23.93	22.94

4. Conclusions

The effects of including Euler/Navier-Stokes calculations in our variable-complexity HSCT design optimization process have been assessed through comparison of CFD and linear theory predictions of the supersonic aerodynamic forces and moments and structural loading of HSCT configurations. The accuracy of the CFD computations and linear theory results was assessed through comparison with experimental data. Euler analysis is more accurate than the Harris wave drag results in its prediction of the wave drag for relatively non-slender forebodies and wings. But for a slender HSCT wing, the results of the two methods were found to match within 1.5 counts for Mach numbers from 1.2 through 3.0. Linear supersonic theory consistently overpredicts the lift coeffi-

cient. The viscous drag predictions from PNS calculations and the algebraic skin friction estimates matched within 2.0 counts for the HSCT wings considered. When the algebraic skin friction estimate was added to the inviscid drag predicted from Euler analyses for these wings, the results differed by only 2 counts at cruise ($C_L = 0.8$). In contrast, the drag at cruise predicted from linear supersonic theory was less than that computed from the PNS equations by as much as 10 counts. This corresponds to a 750 n.mi. overprediction in the range, out of the nominal 5500 n.mi. range of the aircraft, when using linear supersonic theory drag predictions. The pitching moments predicted from PNS, Euler, and linear theory match well for the uncambered HSCT wing, but this agreement becomes worse when cambered wings are considered.

Another significant improvement in moving to CFD comes in the prediction of the distributed loads used in the structural optimization. Euler and PNS calculations capture the details of the pressure variations across the wing better than linear supersonic theory. This is especially true for large angles of attack where the leading-edge singularity in the panel method does not predict the pressures near the leading edge accurately. These errors have a significant effect on the wing stresses and wing bending material weight predictions from structural optimization. The wing bending stresses and structural optimization are very sensitive to changes in the spanwise location of the center of pressure. Differences in the predicted center of pressure location between Euler and linear theory, which are on the order of 1.5 feet on a 74 ft. semi-span wing, can translate to a 20 percent difference in the wing bending stresses and more than a 10 percent difference in the structural weight.

As expected, significant differences in computational effort for HSCT calculations were seen for PNS, Euler and linear theory. For HSCT wings, the PNS calculations took approximately 3 hours, the Euler calculations required 15 minutes, and linear supersonic theory took one second to compute on an SGI Power Challenge XL. The increase in computational effort for CFD calculations will require that only a small number of CFD computations be used to supplement the lower order predictions in our variable-complexity approach to multidisciplinary design optimization. A method must be developed which uses a small number of CFD analyses to update the less accurate and less expensive linear supersonic theory results. Research to achieve this goal through response surface methods[35,36] is currently in progress as part of our MAD Center activities. In the future, we plan to investigate the use of Euler/Navier-Stokes codes for transonic load cases. We expect to see a much larger increase in accuracy from using CFD results for transonic loads, but with a concomitant increase in the computational effort.

Acknowledgment

This work was supported by the NASA Langley Research Center under grants NAG1–1160 and NAG1–1562.

References

[1] Hutchison, M. G., Unger, E. R., Mason, W. H., Grossman, B., and Haftka, R. T., "Aerodynamic Optimization of an HSCT Configuration Using Variable-Complexity Modeling," AIAA Paper No. 93–0101, January 1993.

[2] Hutchison, M. G., Unger, E. R., Mason, W. H., Grossman, B., and Haftka, R. T., "Aerodynamic Optimization of an HSCT Configuration Using Variable-Complexity Modeling," *Journal of Aircraft*, Vol. 31, No. 1, pp. 110-116, 1994.

[3] Dudley, J., Huang, X., Haftka, R. T., Grossman, B., and Mason, W. H., "Variable-Complexity Interlacing of Weight Equation and Structural Optimization of the High-Speed Civil Transport," AIAA Paper No. 94–4377, September 1994.

[4] Dudley, J., Huang, X., MacMillin, P. E., Grossman, B., Haftka, R. T., and Mason, W. H., "Multidisciplinary Optimization of the High-Speed Civil Transport," AIAA Paper No. 95–0124, January 1995.

[5] Harris, R. V.,Jr., "An Analysis and Correlation of Aircraft Wave Drag," NASA TM X–947, 1964.

[6] Carlson, H. W. and Miller, D. S., "Numerical Methods for the Design and Analysis of Wings at Supersonic Speeds," NASA TN D–7713, 1974.

[7] Carlson, H. W. and Mack, R. J., "Estimation of Leading-Edge Thrust for Supersonic Wings of Arbitrary Planforms," NASA TP–1270, 1978.

[8] Hollenback, D. M. and Blom, G. A., "Application of a Parabolized Navier-Stokes Code to an HSCT Configuration and Comparison to Wind Tunnel Test Data," AIAA Paper No. 93–3537, August 1993.

[9] Pittman, J. L., Bonhaus, D. L., Siclari, M. J., and Dollyhigh, S. M., "Euler Analysis of a High-Speed Civil Transport Concept at Mach 3," *Journal of Aircraft*, Vol. 28, No. 4, April 1991, pp. 239–245.

[10] Covell, P., Hernandez, G., Flamm, J., and Rose, O., "Supersonic Aerodynamic Characteristics of a Mach 3 High-Speed Civil Transport Configuration," AIAA Paper No. 90–3210, September 1990.

[11] Mann, Michael J. and Carlson, Harry W., "An Assessment of Current Methods for Drag-Due-To-Lift Minimization at Supersonic Speeds," AIAA Paper No. 91-3302, September 1991.

[12] McGrory, W. D., Slack, D. C., Applebaum, M. P., Walters, R. W., *GASP Version 2.2 Users Manual*, Aerosoft, Inc.

[13] Barger, R. L. and Adams, M. S., "Automatic Computation of Wing-Fuselage Intersection Lines and Fillet Inserts with Fixed-Area Constraint," NASA TM 4406, March 1993.

[14] Barger, R. L., Adams, M. S., and Krisnan, R. R., "Automatic Computation of Euler-Marching and Subsonic Grids for Wing-Fuselage Configurations," NASA TM 4573, July 1994.

[15] Craidon, C. B., "Description of a Digital Computer Program for Airplane Configuration Plots," NASA TM X–2074, 1970.

[16] *GENESIS User Manual*, Version 1.3, Vanderplaats, Miura and Associates, Inc., 5960 Mandarin Avenue, Suite F, Goleta, CA 93117

[17] Burgee, S., Giunta, A. A., Narducci, R., Watson, L. T., Grossman, B., and Haftka, R. T., "A Coarse Grained Variable-Complexity Approach to MDO for HSCT Design", in *Parallel Processing for Scientific Computing*, Bailey, D. H., Bjørstad, P. E., Gilbert, J. R., Mascagni, M. V., Schreiber, R. S., Simon, H. D., Torczon, V. J., and Watson, L. T. (eds.), SIAM, Philadelphia, PA, 1995, pp. 96–101.

[18] Huang, X., Haftka, R. T., Grossman, B., and Mason, W. H., "Comparison of Statistical Weight Equations with Structural Optimization for Supersonic Transport Wings," AIAA Paper No. 94–4379, September 1994.

[19] Sacher, P.W., Bradley, R.G., Jr., and Schmidt, W., "Technical Evaluation Report on the Fluid Dynamics Symposium on Validation of CFD [CP-437]," AGARD AR-257, May 1989.

[20] Bobbitt, P.J., "The Pros and Cons of Code Validation," AIAA Paper No. 88–2535, June 1988.

[21] Aeschliman, D.P., Oberkampf, W.L., and Blottner, F.G., "A Proposed Methodology for Computational Fluid Dynamics Code Verification, Calibration, and Validation," 16^{th} International Congress on Instrumentation in Aerospace Simulation Facilities (ICIASF), July 18-21, 1995, Wright-Patterson AFB, OH.

[22] Melnik, R. E., Siclari, M. J., Barber, T., and Verhoff, A., "A Process for Industry Certification of Physical Simulation Codes," AIAA Paper No. 94–2235, June 1994.

[23] Melnik, R. E., Siclari, M. J., Marconi, F., Barber, T., and Verhoff, A., "An Overview of a Recent Industry Effort at CFD Code Certification," AIAA Paper No. 95–2229, June 1995.

[24] Marconi, F., Siclari, M., Carpenter, G., and Chow, R., "Comparison of TLNS3D Computations with Test Data for a Transport Wing/Simple Body Configuration," AIAA Paper No. 94–2237, June 1994.

[25] Harris, R. V., Jr. and Landrum, E. J., "Drag Characteristics of a series of a Series of Low-Drag Bodies of Revolution at Mach Numbers From 0.6 to 4.0," NASA TN-D 3163, 1965.

[26] Mason, W. H. and Lee, J., "Aerodynamically Blunt Bodies and Sharp Bodies," *Journal of Spacecraft and Rockets*, Vol. 31, No. 3, May–June 1994, pp. 406-413.

[27] Weber, J. and King, C., "Analysis of the Zero-Lift Wave Drag Measured on Delta Wings," Aeronautical Research Counsel Reports and Memoranda No. 3818, 1978.

[28] Advisory Group for Aerospace Research & Development (AGARD), "Test Cases for Inviscid Flow Field Methods," AGARD Advisory Report No. 211, 1985.

[29] Mason, W. H., Siclari, M. J., Miller, D. S., and Pittman, J. L., "A Supersonic Maneuver Wing Designed for Nonlinear Attached Flow," AIAA Paper No. 83–0425, January 1983.

[30] Siclari, M., Visich, M., Cenko, A., Rosen, B., and Mason, W., "An Evaluation of NCOREL, PAN AIR, and W123SC3 for Supersonic Wing Pressures," *Journal of Aircraft*, Vol. 21, No. 10, October 1984, pp. 816–822.

[31] Pittman, J. L., Miller, D. S., and Mason, W. H., "Supersonic, Nonlinear, Attached-Flow Wing Design for High Lift With Experimental Validation," NASA TP–2336, August 1984.

[32] Somer, Simon C. and Short, Barbara J., "Free-Flight Measurements of Turbulent-Boundary-Layer Skin Friction in the Presence of Severe Aerodynamic Heating at Mach Numbers from 2.8 to 7.0," NACA TN 3391, 1955.

[33] Eminton, E., "On the Minimization and Numerical Evaluation of Wave Drag," Royal Aircraft Establishment Report AERO.2564, November 1955.

[34] Carlson, Harry W. and Walkley, Kenneth B., "Numerical Methods and a Computer Program for Subsonic and Supersonic Aerodynamic Design and Analysis of Wings With Attainable Thrust Corrections," NASA CR 3808, 1984.

[35] Giunta, A. A., Narducci, R., Burgee, S., Grossman, B., Mason, W. H., Watson, L. T., and Haftka, R. T., "Variable-Complexity Response Surface Aerodynamic Design of an HSCT Wing," AIAA Paper No. 95–1886, June 1995.

[36] Kaufman, M., Balabanov, V., Burgee, S., Giunta, A. A., Grossman, B., Mason, W. H., Watson, L. T., and Haftka, R. T., "Variable-Complexity Response Surface Approximations for Wing Structural Weight in HSCT Design," AIAA Paper No. 96–0089, January 1996.